Global carbon emission accounting: national-level assessment of wildfire CO_2 emission—a case study of China

Xuehong Gong[1,2], Zeyu Liu[2,3], Jie Tian[2,3], Qiyuan Wang[2,3], Guohui Li[2,3], Zhisheng An[1,2], Yongming Han[2,3*]

[1] State Key Laboratory of Earth Surface Processes and Resource Ecology, Faculty of Geographical Science, Beijing Normal University, Beijing 100875, China
[2] State Key Laboratory of Loess and Quaternary Geology, Institute of Earth Environment, Chinese Academy of Sciences, Xi'an 710061, China
[3] National Observation and Research Station of Regional Ecological Environment Change and Comprehensive Management in the Guanzhong Plain, Xi'an 710061, China

Correspondence to: Yongming Han (yongming@ieecas.cn)

1 Statistical methods

The Mann-Kendall trend test is a non-parametric statistical method widely used for analyzing trends in time series data. This method does not require data to follow a specific distribution, making it particularly suitable for environmental science and meteorology fields. The calculation formula for the Mann-Kendall trend test is as follows:

$$S = \sum_{k=1}^{n-1} \sum_{j=k+1}^{n} sign(x_j - x_k)$$

where n is the total number of data points, x_j and x_k are numerical values in the time series, $\sum_{k=1}^{n-1}\sum_{j=k+1}^{n} sign(x_j - x_k)$ is the sign function of the difference between x_j and x_k. Based on the statistic S, the standardized statistic Z of Mann Kendall can be calculated, as follows:

$$Z(S) = \frac{S - E(S)}{\sqrt{VAR(S)}}$$

where E(S) and VAR(S) are the expected value and variance of the statistical measure S. By using the Z-value, we can determine the trend direction and significance in the time series. When the Z value is greater than the critical value, it indicates a significant upward trend; When the negative value of Z is less than the critical value, it indicates a significant downward trend. If the Z value is near zero, the time series has no significant trend. The significance of the trend is verified through a p-value, which represents the probability that the observed trend is generated by a random process. Commonly used significance levels include 90%, 95%, and 99%.

Spatial autocorrelation analysis usually uses Anselin's Moran's I index and Getis coefficient as basic measures, which can reflect the statistical correlation of specific attribute values in space (Anselin et al.,1995). The calculation formula is as follows:

$$I = \frac{n}{S_0} \times \frac{\sum_{i=1}^{n}\sum_{j=1}^{n} w_{ij}(x_i - \bar{x})(x_j - \bar{x})}{\sum_{i=1}^{n}(x_i - \bar{x})^2}$$

where I is the Global Moran's I index, n is the total number of spatial elements. This study is calculated in units of Chinese prefecture-level cities, which is the total number of Chinese prefecture-level cities. $(x_i - \bar{x})$ and $(x_j - \bar{x})$ are the error between the observed values and the average values of specific attribute values on the ith and jth geographic space units, respectively. x_i is the observed value, which is the CO_2 emissions of each geographic space unit. $\bar{x}$ is the average value of x_i, w_{ij} is the weight matrix for the adjacency relationships between geographical units. The Moran's I index is between -1 and 1. When I>0, it indicates a positive correlation between spatial elements, and when I<0, it indicates a negative correlation between spatial elements; When I=0, it indicates no spatial correlation, meaning that the space is randomly distributed. Similar to Mann Kendall, the calculation results are tested using a z-value.

Spearman correlation coefficient is a non-parametric statistical method used to measure the strength and direction of non-linear relationships between two variables. It is based on the rank of two variables rather than the specific values of the original data, so it has good robustness for datasets that do not meet the assumption of normal distribution or have outliers. When the correlation coefficient is 1, it indicates a perfect positive monotonic relationship between the two variables. The correlation coefficient of -1 signifies a perfect negative monotonic relationship. A correlation coefficient of 0 suggests no monotonic relationship between the two variables. Spearman correlation coefficients are commonly used to process rank data, such as ranking data, or for correlation analysis in small sample sizes where the assumption of normal distribution is difficult to satisfy.

Table S1 CO_2 emission factors of different vegetation cover types in China

Paper	Species	Emission factor（g/kg）
Akagi et al. (2011)	Forest	1710 ± 39
Burling et al. (2011)	Forest	1668 ± 72
Prichard et al. (2020)	Conifer forest	1576 ± 248
Prichard et al. (2020)	Mixed forest	1650 ± 61
Jin et al. (2022)	Forest	1392.54 ± 248.53
Prichard et al. (2020)	Shrub	1708 ± 192
Jin et al. (2022)	Shrub	1487.8 ± 18.05
Akagi et al. (2011)	Savanna	1565 ± 159
Prichard et al. (2020)	Grass	1686 ± 81
Jin et al. (2022)	Grass	1465.84 ± 60.45
Cao et al. (2008)	Wheat	1377 ± 431
Sahai et al. (2007)	Wheat	1130
Zhang et al. (2008)	Wheat	791.3
Wang et al. (2009)	Wheat	911.65 ± 105

Cao et al. (2008)	corn	1327 ± 710
Wei et al. (2012)	corn	959
Wang et al. (2009)	corn	1265.4 ± 91.2
Cao et al. (2008)	rice	1674 ± 452
Zhang et al. (2008)	rice	791 ± 12.5
Wang et al. (2009)	rice	976.8 ± 58.5

Table S2 Main emission regions in high emission years under different vegetation cover types

vegetation cover type	year	Total emissions(Tg)	Main emissions regions	The proportion of major regions in the total emissions of the year
Forest	2003	34.4	Heilongjiang, Inner Mongolia	77.0%
Forest	2008	40.3	Inner Mongolia	50.3%
Shrub	2003	14.0	Yunnan, Inner Mongolia, Heilongjiang	69.9%
Shrub	2010	18.2	Yunnan, Guizhou	87.4%
Grassland	2003	1.7	Inner Mongolia, Heilongjiang	89.9%
Grassland	2008	1.3	Inner Mongolia	72.0%
Cropland	2012	25.4	Anhui	48.4%
Cropland	2014	30.2	Heilongjiang	47.8%
Cropland	2015	22.8	Heilongjiang	57.1%
Cropland	2017	25.8	Heilongjiang	70.0%

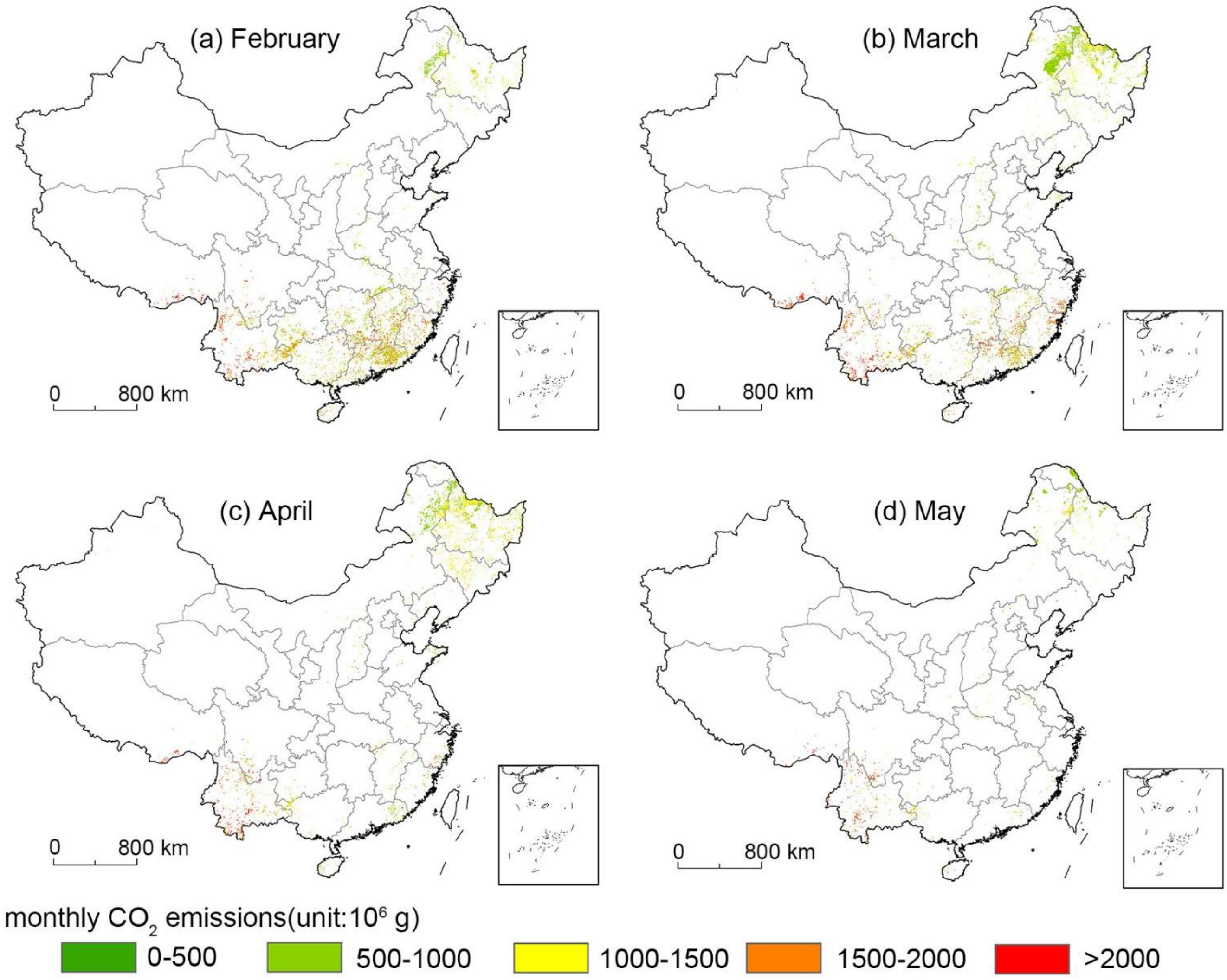

Figure S1: Spatial distribution of monthly CO_2 emissions within forest fires from 2001 to 2022 in China: (a) February, (b) March, (c) April, and (d) May.

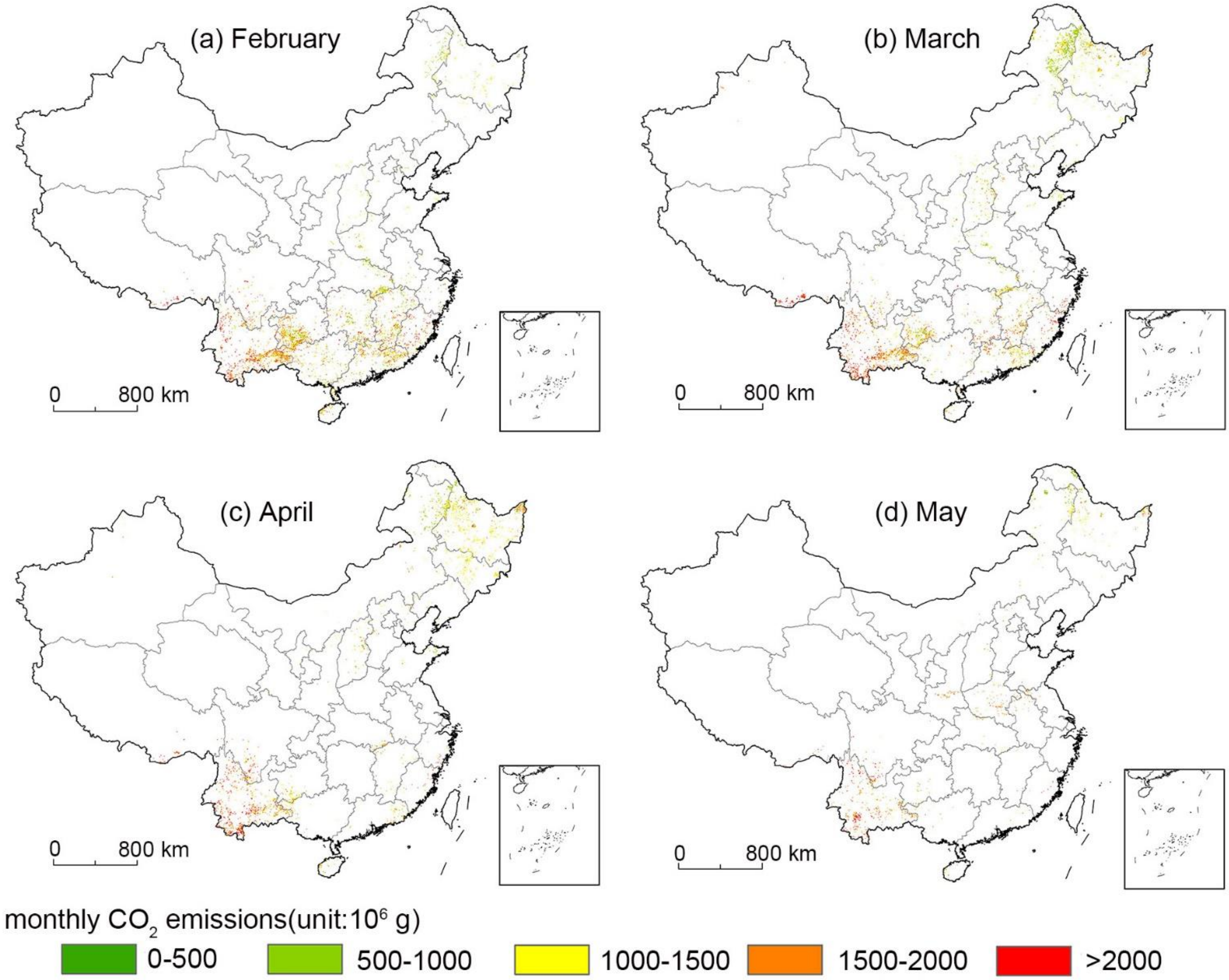

Figure S2: Spatial distribution of monthly CO_2 emissions within shrub fires from 2001 to 2022 in China: (a) February, (b) March, (c) April, and (d) May.

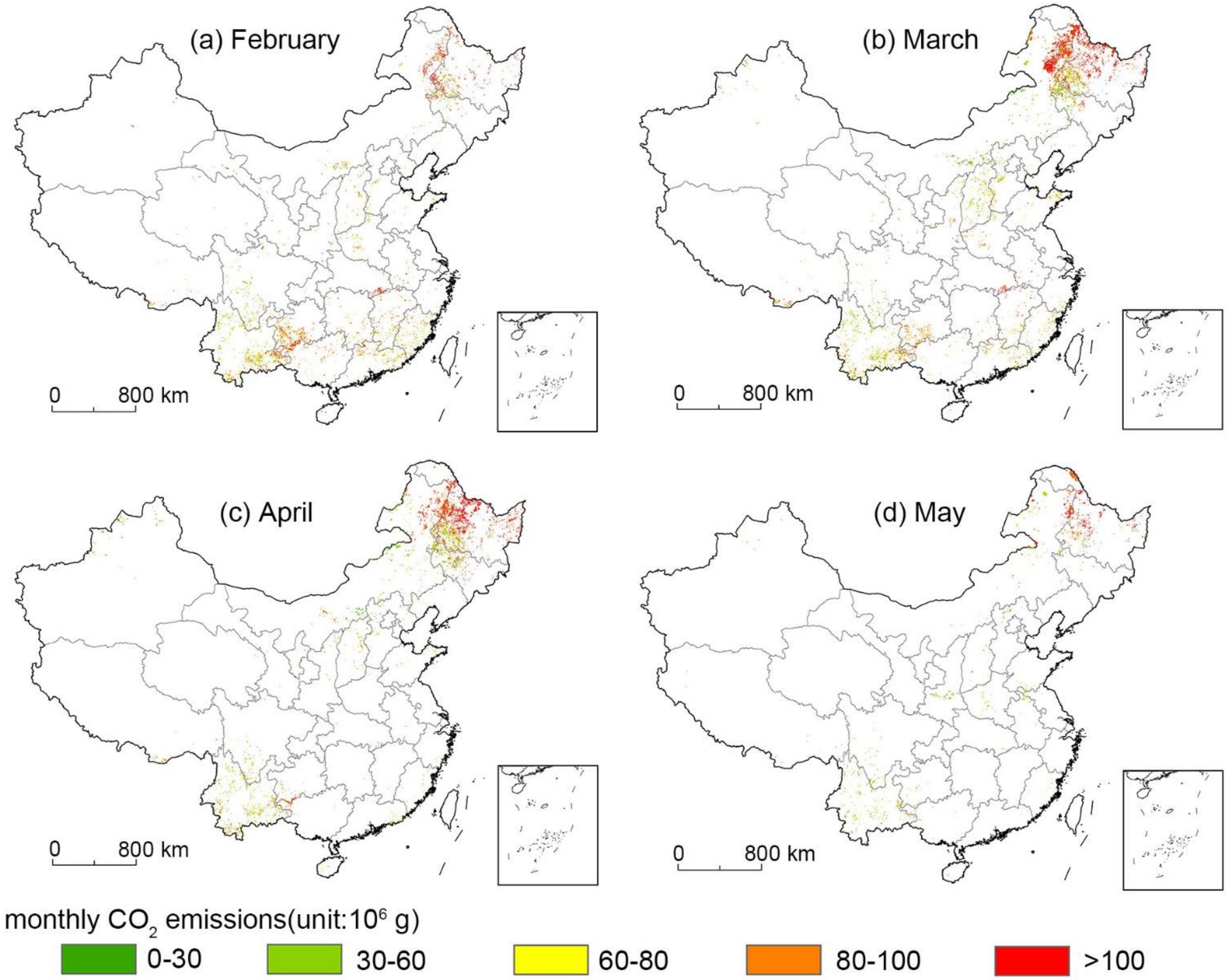

Figure S3: Spatial distribution of monthly CO_2 emissions within grassland fires from 2001 to 2022 in China: (a) February, (b) March, (c) April, and (d) May.

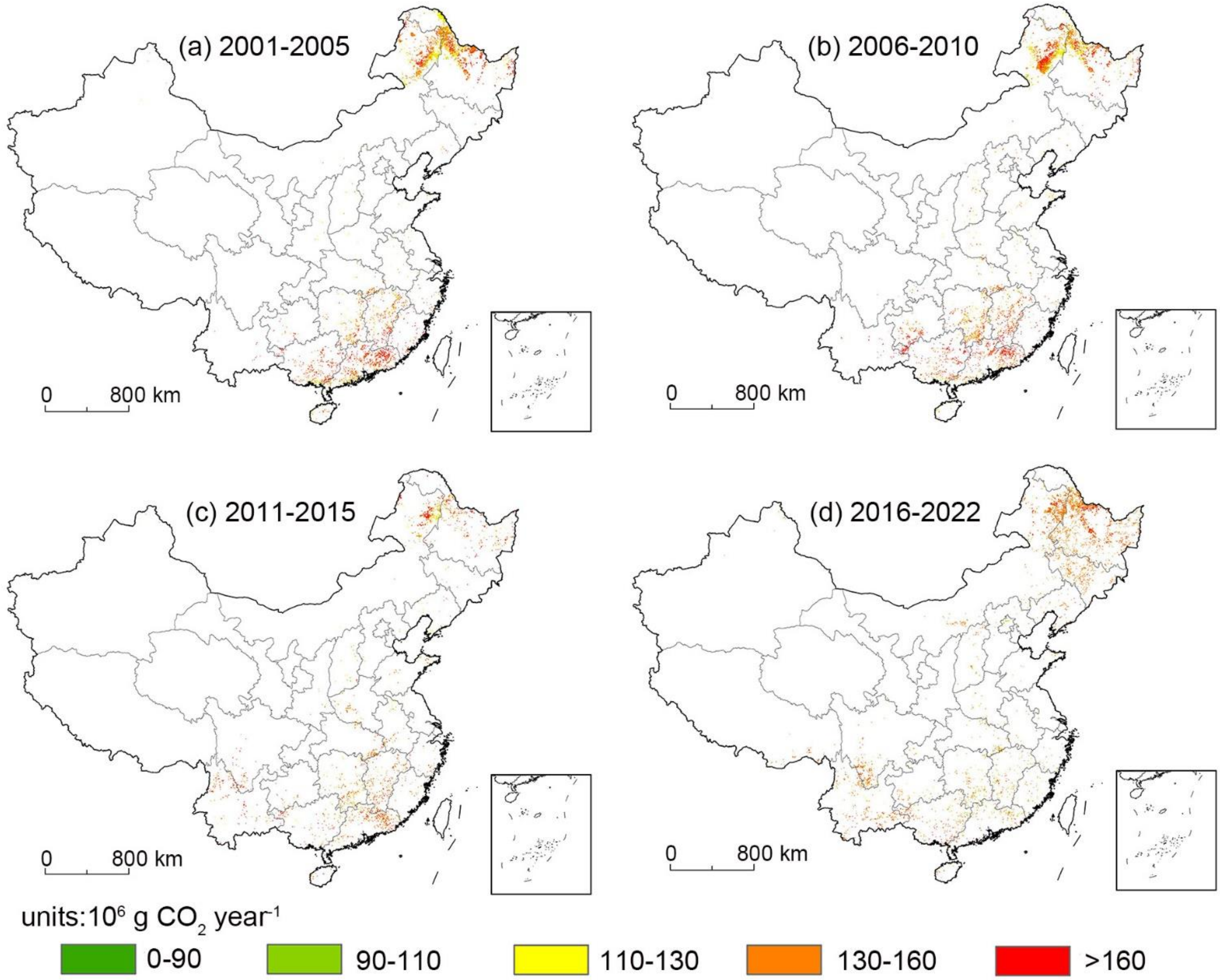

Figure S4: Spatial distribution of annual CO_2 emissions for forest fires from (a) 2001 to 2005, (b) 2005 to 2010, (c) 2011 to 2015, and (d) 2016 to 2022.

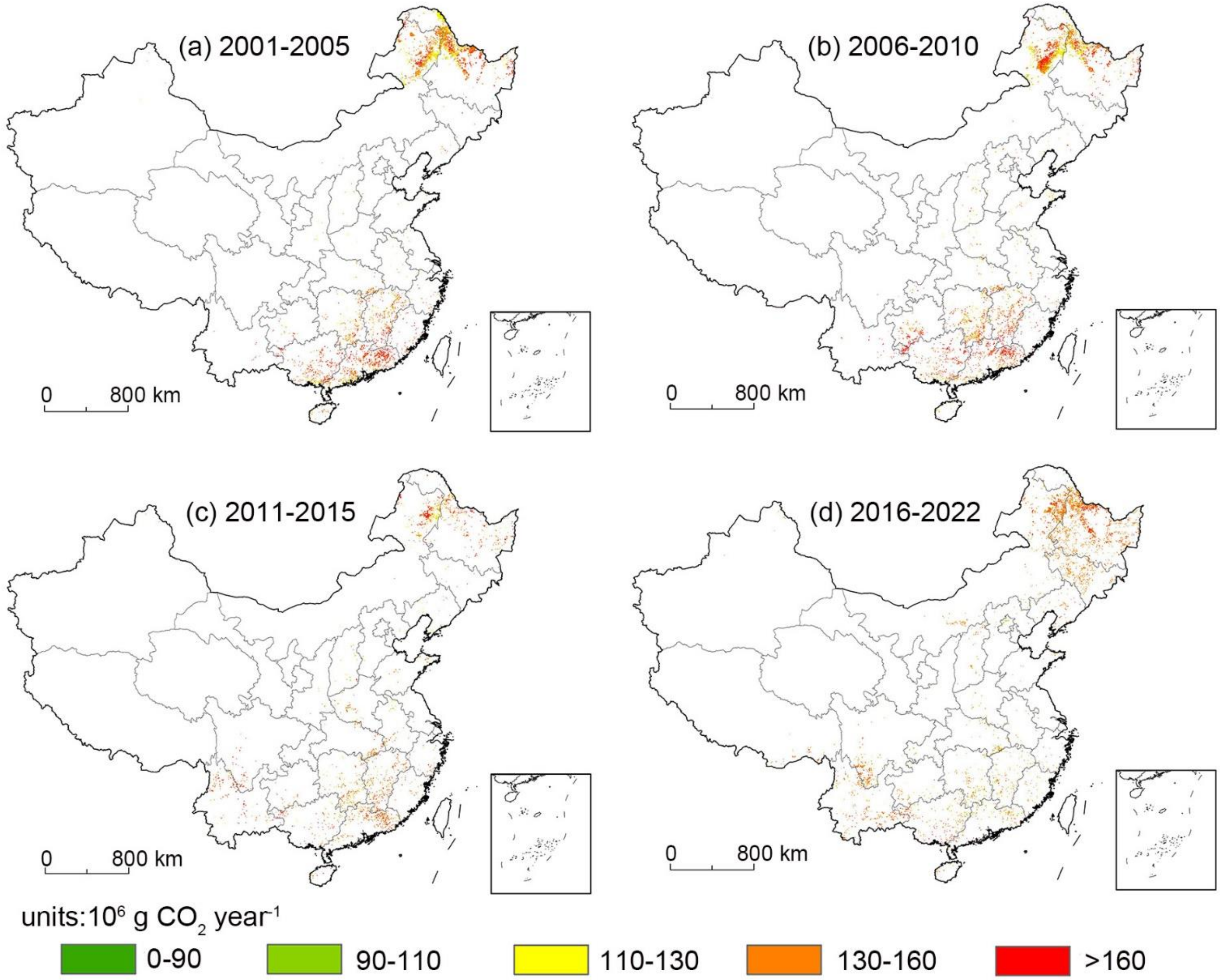

60 **Figure S5: Spatial distribution of annual CO_2 emissions for shrub fires from (a) 2001 to 2005, (b) 2005 to 2010, (c) 2011 to 2015, and (d) 2016 to 2022.**

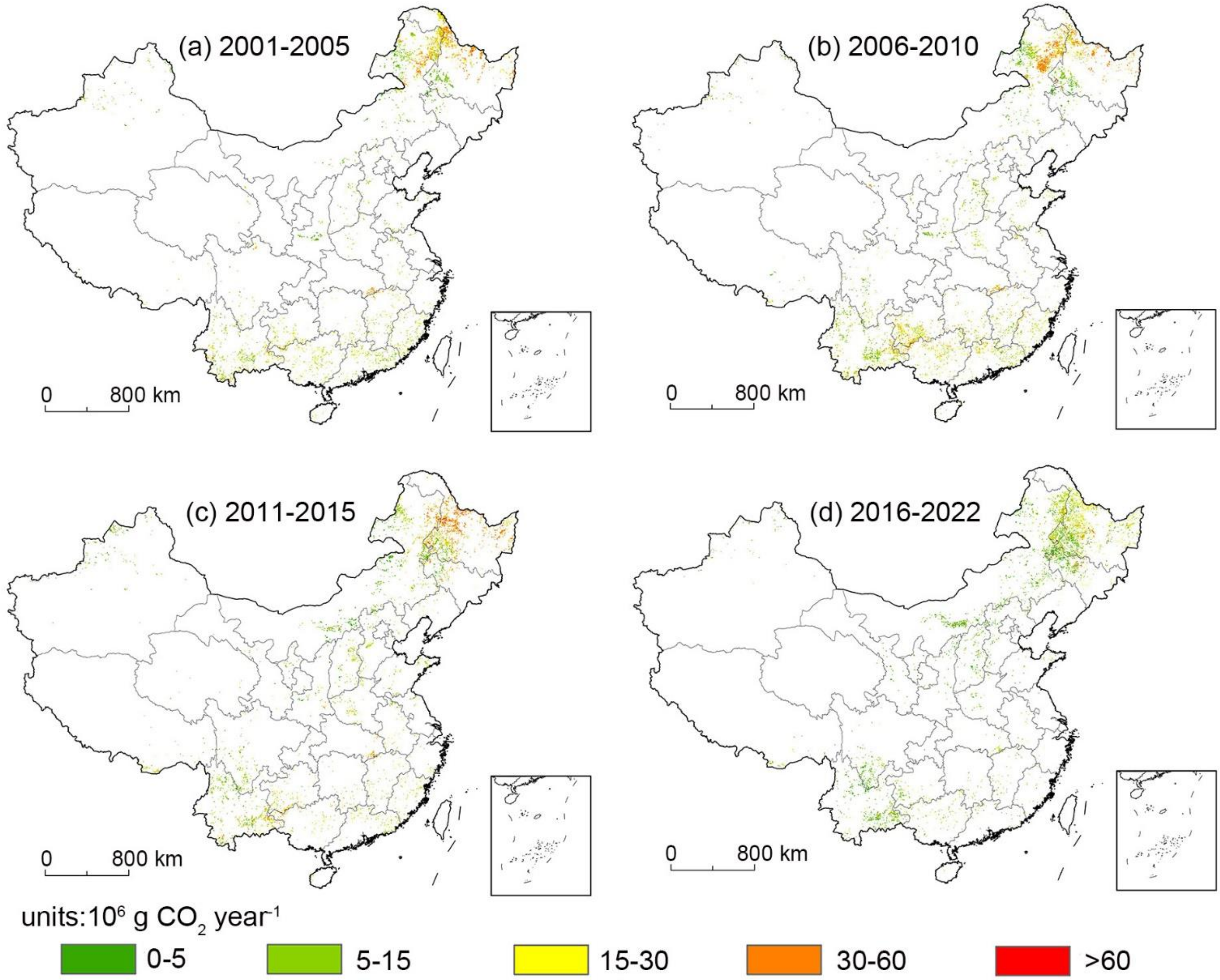

Figure S6: Spatial distribution of annual CO_2 emissions for grassland fires from (a) 2001 to 2005, (b) 2005 to 2010, (c) 2011 to 2015, and (d) 2016 to 2022.

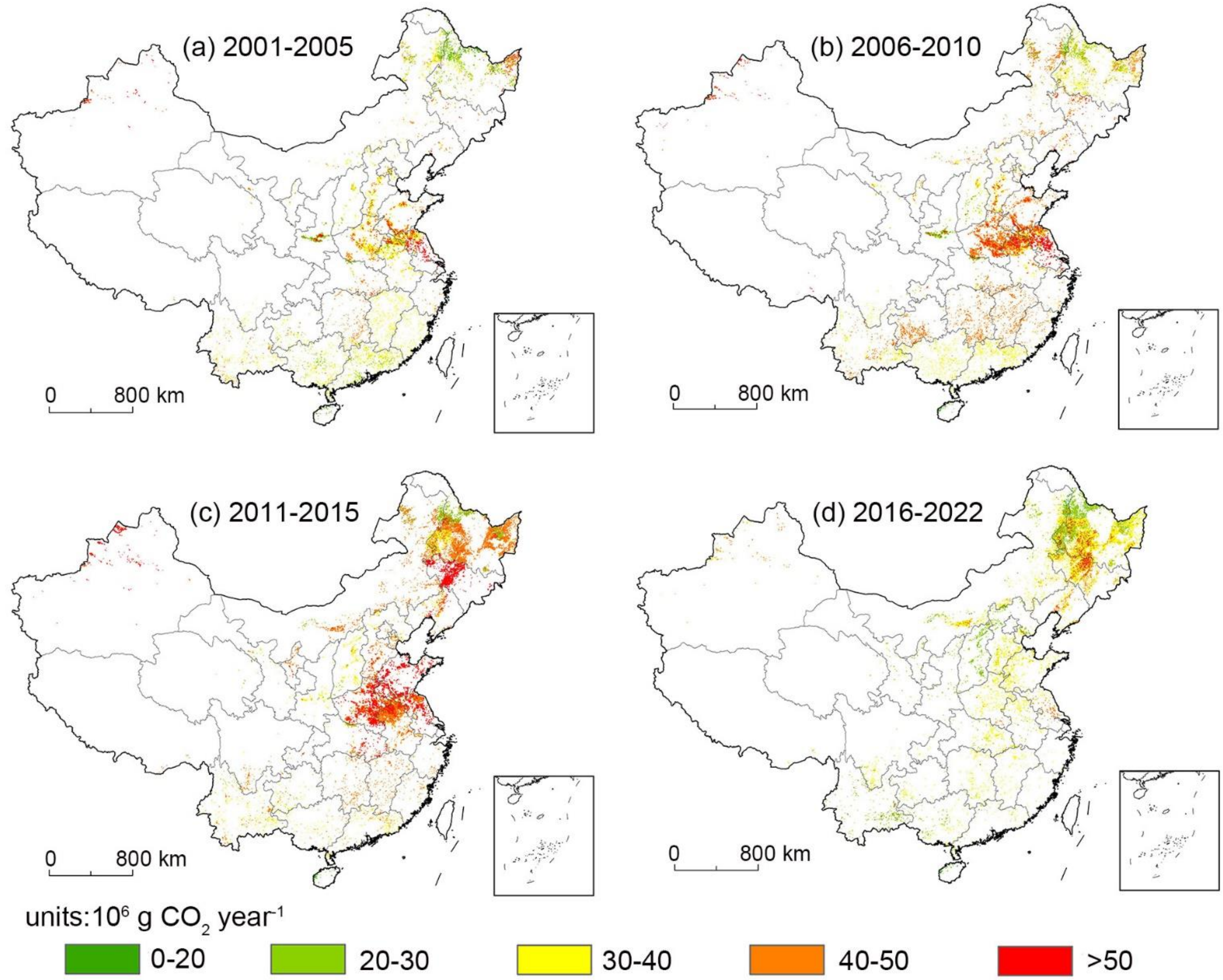

Figure S7: Spatial distribution of annual CO_2 emissions for cropland fires from (a) 2001 to 2005, (b) 2005 to 2010, (c) 2011 to 2015, and (d) 2016 to 2022.

References

Akagi, S. K., Yokelson, R. J., Wiedinmyer, C., Alvarado, M. J., Reid, J. S., Karl, T., Crounse, J. D., and Wennberg, P. O.: Emission factors for open and domestic biomass burning for use in atmospheric models, Atmos. Chem. Phys., 11, 4039–4072, https://doi.org/10.5194/acp-11-4039-2011, 2011.

Anselin, L.: Local Indicators of Spatial Association—LISA, Geogr. Anal., 27, 93–115, https://doi.org/10.1111/j.1538-4632.1995.tb00338.x, 1995.

Burling, I. R., Yokelson, R. J., Akagi, S. K., Urbanski, S. P., Wold, C. E., Griffith, D. W. T., Johnson, T. J., Reardon, J., and Weise, D. R.: Airborne and ground-based measurements of the trace gases and particles emitted by prescribed fires in the United States, Atmos. Chem. Phys., 11, 12197–12216, https://doi.org/10.5194/acp-11-12197-2011, 2011.

Cao, G., Wang, F., and Wang, Y.: Emission inventory of TSP, PM_{10} and $PM_{2.5}$ emissions from biomass burning in China, The Chinese Journal of Process Engineering, 4, 700–704, 2004 (in Chinese).

Jin, Q., Wang, W., Zheng, W., Innes, J. L., Wang, G., and Guo, F.: Dynamics of pollutant emissions from wildfires in Mainland China, J. Environ. Manage., 318, 115499, https://doi.org/10.1016/j.jenvman.2022.115499, 2022.

Prichard, S. J., O'Neill, S. M., Eagle, P., Andreu, A. G., Drye, B., Dubowy, J., Urbanski, S., and Strand, T. M.: Wildland fire emission factors in North America: synthesis of existing data, measurement needs and management applications, Int. J. Wildland Fire, 29, 132, https://doi.org/10.1071/WF19066, 2020.

Sahai, S., Sharma, C., Singh, D. P., Dixit, C. K., Singh, N., Sharma, P., Singh, K., Bhatt, S., Ghude, S., Gupta, V., Gupta, R. K., Tiwari, M. K., Garg, S. C., Mitra, A. P., and Gupta, P. K.: A study for development of emission factors for trace gases and carbonaceous particulate species from in situ burning of wheat straw in agricultural fields in india, Atmos. Environ., 41, 9173–9186, https://doi.org/10.1016/j.atmosenv.2007.07.054, 2007.

Wang, S., Wei, W., Du, L., Li, G., and Hao, J.: Characteristics of gaseous pollutants from biofuel-stoves in rural China, Atmos. Environ., 43, 4148–4154, https://doi.org/10.1016/j.atmosenv.2009.05.040, 2009.

Wei, W., Zhang, W., Hu, D., Ou, L., Tong, Y., Shen, G., Shen, H., and Wang, X.: Emissions of carbon monoxide and carbon dioxide from uncompressed and pelletized biomass fuel burning in typical household stoves in China, Atmos. Environ., 56, 136–142, https://doi.org/10.1016/j.atmosenv.2012.03.060, 2012.

Zhang, H., Ye, X., Cheng, T., Chen, J., Yang, X., Wang, L., and Zhang, R.: A laboratory study of agricultural crop residue combustion in China: Emission factors and emission inventory, Atmos. Environ., 42, 8432–8441, https://doi.org/10.1016/j.atmosenv.2008.08.015, 2008.